

## Article

# Multi-mJ Scaling of 5-Optical Cycle, 3 $\mu\text{m}$ OPCPA

Joana Alves <sup>1,\*</sup> , Hugo Pires <sup>1</sup> , Celso P. João <sup>1,2</sup> and Gonçalo Figueira <sup>1</sup>

<sup>1</sup> Group of Lasers and Plasmas (GoLP), Instituto de Plasmas e Fusão Nuclear (IPFN), Instituto Superior Técnico, Universidade de Lisboa, Av. Rovisco Pais, 1049-001 Lisbon, Portugal; hugo.pires@tecnico.ulisboa.pt (H.P.); celsopaivajoao@tecnico.ulisboa.pt (C.P.J.); goncalo.figueira@tecnico.ulisboa.pt (G.F.)

<sup>2</sup> LaserLeap Technologies, Rua Coronel Júlio Veiga Simão, CTCV, Edifício B, 3025-307 Coimbra, Portugal

\* Correspondence: joanacasanova@tecnico.ulisboa.pt

**Abstract:** We present the design of an ultrafast optical parametric chirped pulse amplifier (OPCPA) operating at 3  $\mu\text{m}$  yielding few-cycle pulses and multi-mJ output energy. This design demonstrates that with a configuration of a single crystal or combination of crystals (KTA and MgO:LN) it is possible to achieve output energies above the mJ with sufficient bandwidth to allow compression to just 5-optical cycles. Here, we consider a 1  $\mu\text{m}$  mJ-level picosecond chirped pulse amplifier (CPA), a typical pumping source for this type of non-linear amplifiers. Compression with a simple bulk material enables reaching close to the pulse Fourier-transform limited duration, paving the way to high energy, ultrafast mid-infrared pulses.

**Keywords:** mid-infrared; ultrafast lasers; parametric amplification; non-linear optics; materials



**Citation:** Alves, J.; Pires, H.; João, C.P.; Figueira, G. Multi-mJ Scaling of 5-Optical Cycle, 3  $\mu\text{m}$  OPCPA. *Photonics* **2021**, *8*, 503. <https://doi.org/10.3390/photonics8110503>

Received: 15 October 2021

Accepted: 4 November 2021

Published: 9 November 2021

**Publisher's Note:** MDPI stays neutral with regard to jurisdictional claims in published maps and institutional affiliations.



**Copyright:** © 2021 by the authors. Licensee MDPI, Basel, Switzerland. This article is an open access article distributed under the terms and conditions of the Creative Commons Attribution (CC BY) license (<https://creativecommons.org/licenses/by/4.0/>).

## 1. Introduction

Ultrafast and broadband laser sources in the mid-IR spectral domain (2–10  $\mu\text{m}$ ) have become highly sought after in the last decade [1], motivated by their wide range of applications in biomedical science, time-resolved spectroscopy, molecular fingerprinting, condensed matter, and, particularly, in strong-field physics with impact in high harmonic generation in gases and solids, X-ray sources, attosecond science and laser wakefield acceleration [2–7]. The interest in these sources is greatly due to the scaling dependence of the ponderomotive potential with  $\sim\lambda^2$ , evidencing the extension of the cut-off photon energy with the increase in the driving wavelength. X-ray supercontinuum generation spanning from the extreme ultraviolet to 1.6 keV was already achieved with such mid-IR pulses, supporting a Fourier-transform limited duration (FTL) of 2.5 as [2].

Extension of the cut-off energy to the keV region has shown to require operation at wavelengths  $\gtrsim 3 \mu\text{m}$ . However, the efficiency of high harmonic generation decreases significantly for longer wavelengths, with a  $\sim\lambda^{-(5-6)}$  factor, due to the scaling of the single-atom yield. This sets the 3  $\mu\text{m}$  driving wavelength as a good compromise for a mid-IR laser, being at the same time conveniently slightly above the water absorption peak at  $\sim 2.8 \mu\text{m}$ . The scarcity of ultrafast solid-state lasers in this spectral range limits the generation of energetic ultrashort mid-IR pulses to non-linear techniques, such as optical parametric chirped pulse amplification (OPCPA) [8]. There are other techniques that can provide 3  $\mu\text{m}$  ultrafast pulses at very high-repetition rates ( $> \text{MHz}$ ), however they are still limited to the ps-regime and nJ-level [9,10]. A typical 3  $\mu\text{m}$ , high-repetition rate, sub-mJ-level OPCPA system is pumped at 1  $\mu\text{m}$  by a mJ-level picosecond diode-pumped source. A fraction of the pump is used to generate a nJ-level supercontinuum in a bulk material, ensuring the tight pump-to-signal synchronization. This is followed by 3–4 optical parametric amplification stages and bulk compression, leading to few-cycle,  $\mu\text{J}$ -level output pulses with high quality and signal-to-noise contrast.

Most of the current mid-IR sources in this wavelength range operate at high (50–100 kHz or above) repetition rates and high stability. Although these characteristics

are ideal for the research of processes with low cross sections, energies below the mJ-level are not optimal for driving low-efficiency processes, such as soft X-ray high harmonic generation and for efficient laser wakefield acceleration, making the scaling in energy of the mid-IR pulses a highly promising and rewarding challenge. Existing state-of-the-art OPCPA systems operating at 3  $\mu\text{m}$  can broadly be grouped into two classes: (i) high repetition rate sources ( $\geq 100$  kHz) that operate at the multi- $\mu\text{J}$ -level, with the main reference systems at ICFO (131  $\mu\text{J}$ , 97 fs, 160 kHz), ELI Alps (152  $\mu\text{J}$ , 38 fs, 100 kHz), MBI Berlin (30  $\mu\text{J}$ , 70 fs, 100 kHz), and CELIA (8  $\mu\text{J}$ , 85 fs, 100 kHz) [11–14], and (ii) a very limited group with sources that can operate close or at the mJ-level but at lower (10–10,000 Hz) repetition rates, with the main reference systems at RIKEN (21 mJ, 70 fs, 10 Hz), Shanghai (13.3 mJ, 111 fs, 10 Hz), Singapore (2.7 mJ, 50 fs, 10 kHz), JILA (0.85 mJ, 420 fs, 1 kHz), and CAS Beijing (0.52 mJ, 100 fs, 1 kHz) [15–19]. State-of-the-art, high repetition rate mid-IR sources usually rely on periodically-poled lithium niobate (PPLN) for the non-linear medium [11,12,18] while mJ-level systems use mainly bulk material crystals, such as lithium niobate (LiNbO<sub>3</sub>, LN) [15,16] and potassium titanyl arsenate (KTiOAsO<sub>4</sub>, KTA) [20,21] (although in the latter case the output is already closer to 4  $\mu\text{m}$ ), clearly evidencing the potential of these crystals in withstanding and operating at high optical intensity levels.

Scaling of the  $\sim 50$   $\mu\text{J}$ ,  $\sim 50$  fs,  $\sim \text{GW}$  output pulses typically provided by the systems in the first group above by almost 2 orders of magnitude is not trivial. The most efficient approach is through OPCPA and the use of an energetic pump source synchronized with the seed. Here, ytterbium-doped (Yb-doped) solid-state lasers, a well established 1  $\mu\text{m}$  technology, are particularly suitable for 3  $\mu\text{m}$  OPCPA pumping due to the good phase matching conditions, their high efficiency and high peak powers [22,23], allowing high repetition rate operation and higher quantum efficiency. Furthermore, in order to preserve the broad bandwidth a careful choice of the mid-IR optical materials is essential. In particular, the use of high aperture, high damage-threshold non-linear crystals capable of supporting amplification over ultrabroad bandwidths in the mid-IR is essential.

Here we analyze in detail, through numerical simulations, the performance of several non-linear crystals in an OPCPA configuration with the goal of achieving 3  $\mu\text{m}$ , mJ-level, few-cycle output pulses. In particular, we propose the individual and combined use of two non-linear crystals, potassium titanyl arsenate (KTA) and magnesium oxide doped lithium niobate (MgO:LiNbO<sub>3</sub>, MgO:LN), as an ultrabroadband mechanism for the optical parametric amplification of 3  $\mu\text{m}$  pulses from the  $\mu\text{J}$  up to the mJ-level pumped by 1  $\mu\text{m}$  sources. We study a range of configurations and compare their outputs in terms of amplified bandwidth, efficiency, and total gain. We find that by using a single 60 mJ, 6 ps ytterbium-based pump source at 1030 nm it is possible to obtain an output energy in excess of 5 mJ. We also show that these pulses can be compressed to 5-optical cycles by using compact bulk compression. The numerical model used is a powerful tool that allows the simulation of the relevant nonlinear phenomena involved in the amplification process in the spatial and temporal dimensions [24].

## 2. Choice of Non-Linear Crystals and Simulation Parameters

### 2.1. Mid-IR Materials for 3 $\mu\text{m}$ Amplification Pumped at 1 $\mu\text{m}$

Currently, the availability of non-linear materials transparent to both the seed ( $\sim 3$   $\mu\text{m}$ ) and pump ( $\sim 1$   $\mu\text{m}$ ) wavelengths, allowing broad phasematching conditions and exhibiting a high laser-induced damage threshold (LIDT) is scarce. Among those, we have KTA, a positive biaxial crystal with high LIDT ( $> 200$  GW/cm<sup>2</sup> at 740–840 nm, 0.2 ps, 1 kHz [25]), an approximately constant spectral transmission in the range  $\sim 0.5$ – $3.5$   $\mu\text{m}$  and moderate non-linear coefficient ( $d_{\text{eff}} \sim 2.1$  pm/V). Additionally, KTA allows collinear amplification, enabling a simpler design, operation, and less beam aberrations, making it ideal for OPCPA. Potassium titanyl phosphate (KTiOPO<sub>4</sub>, KTP) [25] is a material from the same family as KTA showing the same high LIDT. However, its decreasing transmission at 3  $\mu\text{m}$  makes it less desirable for amplification in this region.

Potassium niobate (KNbO<sub>3</sub>, KN) is a negative biaxial crystal from a different family, for which a LIDT as high as that of KTA has been reported (>200 GW/cm<sup>2</sup> at 800 nm, 0.2 ps, 1 kHz [26]), while also exhibiting a high non-linear coefficient ( $d_{\text{eff}} = 6.0$  pm/V) and allowing for a broad phase-matched bandwidth in non-collinear geometries. An experimental study performed with KN crystal for amplification at 3.15  $\mu\text{m}$  with 370 nm bandwidth at  $1/e^2$  has demonstrated its broadband amplification capability while also showing that at intensities larger than 14.4 GW/cm<sup>2</sup> for 9.5 ps, 160 kHz, 1064 nm pulses led to optical damage [27]. Furthermore, this material is prone to multi-domain issues due to its structural and ferroelectric properties requiring careful operation.

A more suitable material with particular interesting properties for mJ-scaling is lithium niobate (LiNbO<sub>3</sub>, LN), a crystal with negative uniaxial birefringence which when doped with magnesium oxide (MgO) can further reduce the green-induced infrared absorption (GRIIRA) [28]. Its structural type (congruent and stoichiometric) and doping concentration might slightly vary the LIDT of the crystal, but 5 mol% MgO-doped congruent LN was recently reported to have an LIDT comparable to KTA ( $204 \pm 4$  GW/cm<sup>2</sup>, 10 kHz, 1 ps, 1030 nm) [29]. A recent publication reported that MgO:LN could withstand powers as high as 25 GW/cm<sup>2</sup> at 800 nm, 10 Hz, 6.6 ps in an OPCPA configuration [15]. Furthermore, MgO:LN has a high non-linear coefficient ( $d_{\text{eff}} \sim 3.9$  pm/V) allowing for large phase matching bandwidth which together with its high to moderate LIDT value makes it a very promising crystal for ultrabroadband mJ-level amplification. This material is also used in a periodically poled configuration (PPLN). On the one hand, this brings the advantage of quasi-phase matching (QPM), but on the other hand it has represented so far a challenge for high pumping power, and, therefore, to mJ-scaling, due to parasitic interactions and thermal effects. For this reason, PPLNs are not considered in the present work. Table 1 summarizes the relevant properties of the crystals of interest for high-energy amplification at 3  $\mu\text{m}$  as discussed above, as well as their calculated acceptance bandwidth (assuming a crystal length of  $L = 2$  mm) for operation at the wavelength in question.

**Table 1.** Relevant optical properties of MgO:LN, KN and KTA for high power parametric amplification. The bandwidth shown is calculated for a  $L = 2$  mm crystal.

| Crystal | $d_{\text{eff}}$ (pm/V) | LIDT (GW/cm <sup>2</sup> )               | Bandwidth (nm)  |
|---------|-------------------------|--|---|
| MgO:LN  | 3.9                     | $204 \pm 4$ (1030 nm, 10 kHz, 1 ps) [15] | 495 (Type I, $\theta = 40.3^\circ$ , $\alpha = 5^\circ$ )   |
| KN      | 6.0                     | >14.4 (1064 nm, 160 kHz, 9.5 ps) [27]    | 670 (Type I, $\theta = 40.7^\circ$ , $\alpha = 4.5^\circ$ ) |
| KTA     | 2.1                     | >200 (740–840 nm, 1 kHz, 0.2 ps) [25]    | 208 (Type II, $\theta = 41.6^\circ$ )                       |

## 2.2. Amplification Parameters and Numerical Model

For our numerical model we chose a set of initial parameters typical of the laser systems as described above: a 3.05  $\mu\text{m}$ , 50 fs (FTL), 50  $\mu\text{J}$  pulse was set as the initial signal for amplification. For the pump we considered parameters typical of an Yb-doped, multipass, CPA type system, with a 500 fs pulse stretched to 6 ps, and a maximum available energy of 100 mJ at 1030 nm. This stretched pulse duration allows the amplification of a 2 ps signal while avoiding gain narrowing and enabling compact straightforward bulk compression of the amplified pulse. The signal pulse is, therefore, assumed to be chirped and stretched to this duration. The maximum beam radius at  $1/e^2$  was set to 2.5 mm, which was considered for a compact configuration and well below the current size limit of homogeneous KTA crystals ( $\sim 15 \times 15$  mm<sup>2</sup>). The pump energy was limited by the maximum radius and pulse duration with respect to the damage threshold of each crystal. Both beams were considered to have spatially Gaussian profiles.

The numerical simulation of the relevant non-linear phenomena involved in the OPCPA amplification process and comprehensive data were obtained through the use of the chi2D software [24]. This numerical 2 + 1 dimensional model takes into account second-order non-linear interactions in birefringent media with only two coupled differential equations relative to the ordinary and extraordinary fields, which distinguishes it from the

three coupled equations split-step Fourier methods for pump, signal, and idler, allowing for moderate computing times on standard desktop computers without substantial loss of accuracy. With this software, single and multiple non-linear stages, as well as their stretching and compression, were studied for achieving the best compromise between final number of cycles and energy.

### 3. Results

#### 3.1. Single OPCPA Stage

The simpler configuration that allows achieving the mJ-level consists in a single-stage, KTA-based OPCPA pumped at  $63.8 \text{ GW/cm}^2$  (pump energy is 40 mJ). The corresponding optimum phase matching angle and crystal length are  $\theta = 41.6^\circ$ , Type II interaction ( $d_{\text{eff}} = 2.1 \text{ pm/V}$ ) for a 2.5 mm long crystal. The choice of length stems from a compromise between maximum energy and minimal duration while preserving the beam quality (indicated by the  $M^2$  factor), see Figure 1 and Table 2. For these parameters, output pulses with 1.92 mJ, 74 fs at 3130 nm central wavelength were obtained. This represents an overall gain of 38.4 and a 4.8% pump-to-signal conversion efficiency. However, the simple setup comes at the cost of an undesirable pulse broadening factor of 48%, which nevertheless allows compression to just 7-optical cycles. Figure 1 shows the output energy, compressed pulse duration, pulse spectrum and spatiotemporal profile for the parameters studied.

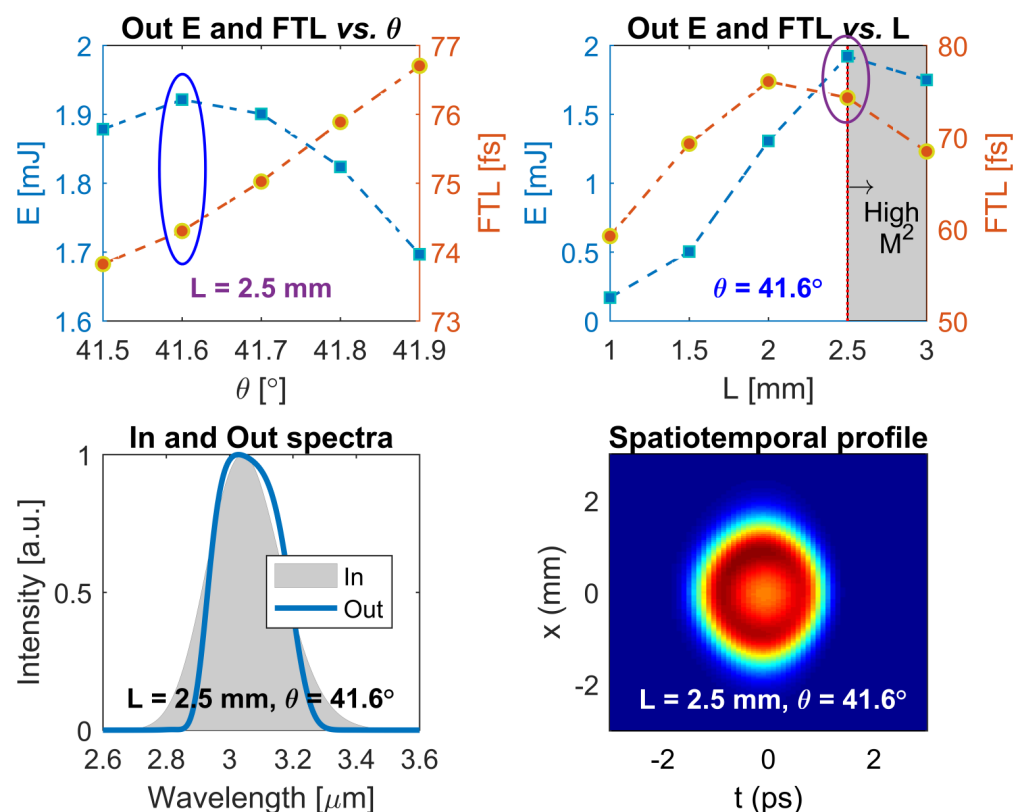


**Figure 1.** Results for a single collinear KTA-based amplification stage. **Top:** output energy and compressed pulse duration vs. **(left)** phase matching angle  $\theta$  for  $L = 2.5 \text{ mm}$  and **(right)** crystal length  $L$  for  $\theta = 41.6^\circ$ . The circled points mark the optimum combination of both parameters. **Bottom left:** Input (**shaded**) and output (**blue**) spectra for the optimal parameters. **Bottom right:** Spatiotemporal profile of the optimized output pulse with 1.92 mJ and 74 fs (FTL).

The single stage configuration was also studied for MgO:LN. Although recent LIDT studies show that this material could allow intensities similar to those of KTA [29], we have limited this parameter to the conservative value ( $25 \text{ GW/cm}^2$ ) used in an OPCPA configuration [15] as stated earlier. This is equivalent to using a maximum pump energy of

16 mJ. For this case, the optimum phase matching angle is  $46.7^\circ$  for a Type I non-collinear geometry with a  $5.1^\circ$  angle in the XZ plane, for which we have ( $d_{\text{eff}} = 3.9 \text{ pm/V}$ ), and a crystal length of 2.3 mm. For these parameters, output pulses with 1.12 mJ, 51 fs at 3054 nm central wavelength were obtained. This represents a gain of 22.4 and a pump to signal efficiency of 7.0%. It is clear that the non-collinear geometry is highly favorable in terms of bandwidth, with the signal spectrum being preserved, corresponding to a 5-cycle duration. Figure 2 plots the same parameters as above for the case of MgO:LN.

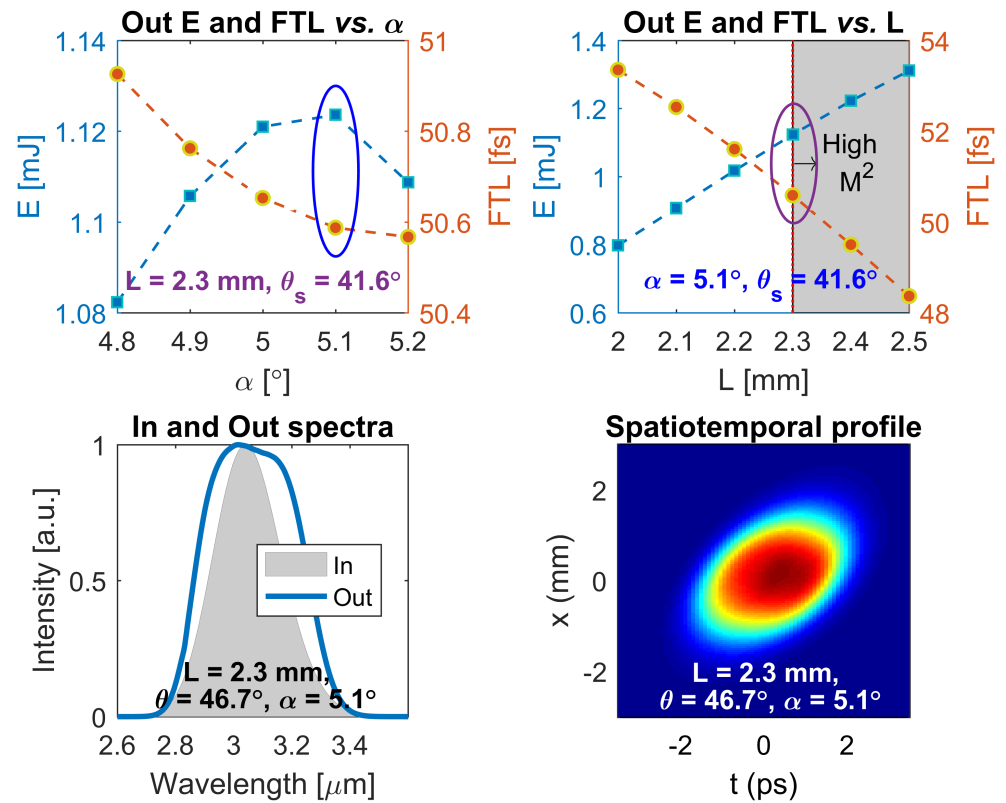


**Figure 2.** Results for a single non-collinear MgO:LN-based amplification stage. (Top) output energy and compressed pulse duration vs. (left) non-collinear angle  $\alpha$  for  $L = 2.3 \text{ mm}$  and (right) crystal length  $L$  for  $\alpha = 5.1^\circ$ . The circled points mark the optimum combination of both parameters. (Bottom left) Input (shaded) and output (blue) spectra for the optimal parameters. (Bottom right) Spatiotemporal profile of the optimized output pulse with 1.12 mJ and 51 fs (FTL).

**Table 2.** Amplification parameters and output values of the proposed single KTA and MgO:LN OPCPA configurations for few-cycle, mJ-level.

| Single OPCPA          | Stage  |      |
|-----------------------|--------|------|
|                       | MgO:LN | KTA  |
| Crystal               | MgO:LN | KTA  |
| Pump (mJ)             | 16     | 40   |
| Radius (mm)           | 2.5    | 2.5  |
| Length (mm)           | 2.3    | 2.5  |
| $\theta$ ( $^\circ$ ) | 46.7   | 41.6 |
| $\alpha$ ( $^\circ$ ) | 5.1    | -    |
| Out $\lambda_c$ (nm)  | 3054   | 3130 |
| Out energy (mJ)       | 1.12   | 1.92 |
| Out FTL (fs)          | 51     | 74   |
| Out cycles            | 5      | 7    |
| Eff conversion (%)    | 7.0    | 4.8  |
| Gain                  | 22.4   | 38.4 |

### 3.2. Multiple OPCPA Stages

A different approach consists in modelling the crystal amplification performance for lower gain, but with multiple OPCPA stages. For this case, we considered a pump intensity of  $6.4 \text{ GW/cm}^2$  (pump energy  $4 \text{ mJ}$ ), one-tenth of the previously used value. KTA still shows bandwidth narrowing and pulse broadening, with the output energy and spectrum depending strongly on the crystal thickness. For a  $2 \text{ mm}$  long crystal the spectral width narrows by  $\sim 25\%$  but the energy ( $69.7 \mu\text{J}$ ) is not optimal. The maximum energy output ( $144.4 \mu\text{J}$ ) is obtained for  $L = 5.3 \text{ mm}$  but with significant bandwidth narrowing. These results make KTA unsuitable for the lower energy amplification stages. The same pump intensity applied to MgO:LN allows preserving the FTL duration ( $53 \text{ fs}$ ) with an optimal pump-to-signal conversion efficiency of  $7.4\%$ , corresponding to  $347.7 \mu\text{J}$ , 5 cycles. The optimal crystal length was of  $3.6 \text{ mm}$ . Figure 3 summarizes these results.

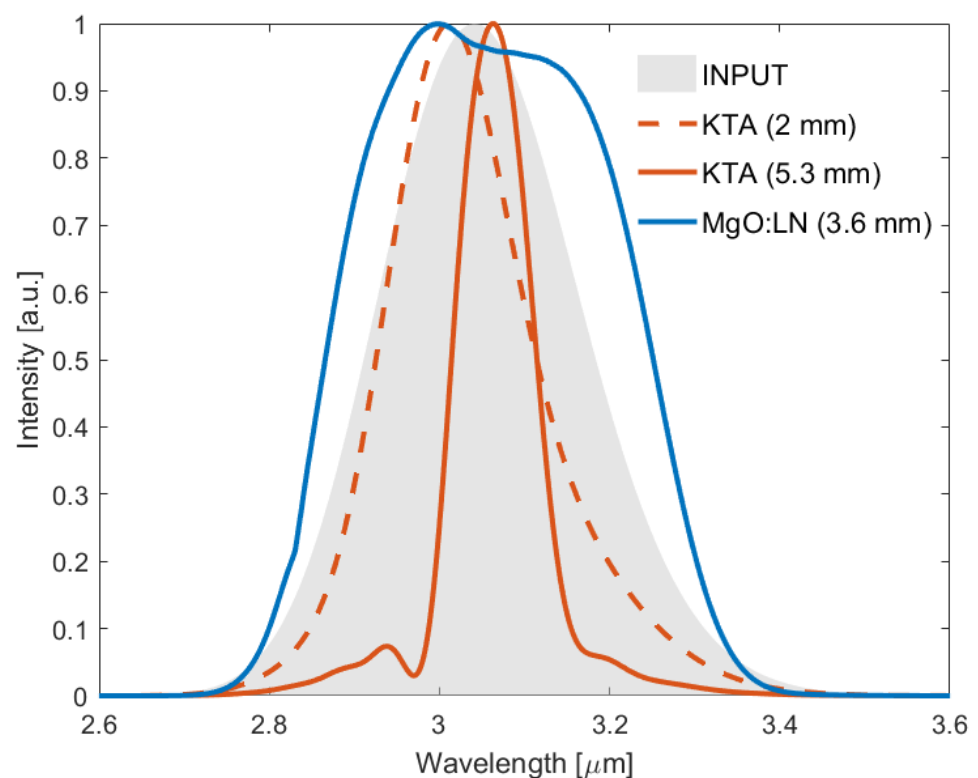


**Figure 3.** Output spectra for a  $4 \text{ mJ}$  pump. Input signal (shaded curve),  $2 \text{ mm}$  long KTA (dashed red),  $5.3 \text{ mm}$  long KTA (red), and  $3.6 \text{ mm}$  long MgO:LN (blue).

Having confirmed the suitability of MgO:LN for the low energy stages, next we explore a combination of crystals in the search for an ideal configuration for multi-mJ, few-cycle output. For this, we scale further the output pulse from this stage (OPA 1) with a second non-collinear MgO:LN stage (OPA 2). Considering the same limit intensity for MgO:LN as previously ( $16 \text{ mJ}$ ,  $25 \text{ GW/cm}^2$ ), this double-stage OPCPA delivers 5-cycle,  $2.06 \text{ mJ}$  pulses for an optimal crystal length of  $2 \text{ mm}$ , already at the few-mJ-level, few-cycle regime. In order to scale this output even further to the multi-mJ, a third stage can be added to this setup. Using MgO:LN again would be of interest, provided higher pump intensities could be used. Instead, and keeping with the conservative approach, we consider a high-energy, KTA-based stage. This approach combines efficiently the large phase-matched amplification bandwidth and high non-linear coefficient of MgO:LN in a first non-collinear double-stage and the high LIDT of KTA for the third one in a collinear configuration. Pumping this stage with  $40 \text{ mJ}$ , yields an optimal crystal length of  $1.4 \text{ mm}$ , generating 5-cycle,  $5 \text{ mJ}$  pulses. Figure 4 shows the amplified bandwidth of the proposed design and Table 3 lists the main parameters for each stage. This output energy represents

a net gain factor of 100 and 8.4% pump to signal conversion efficiency, for a total pump energy of 60 mJ.

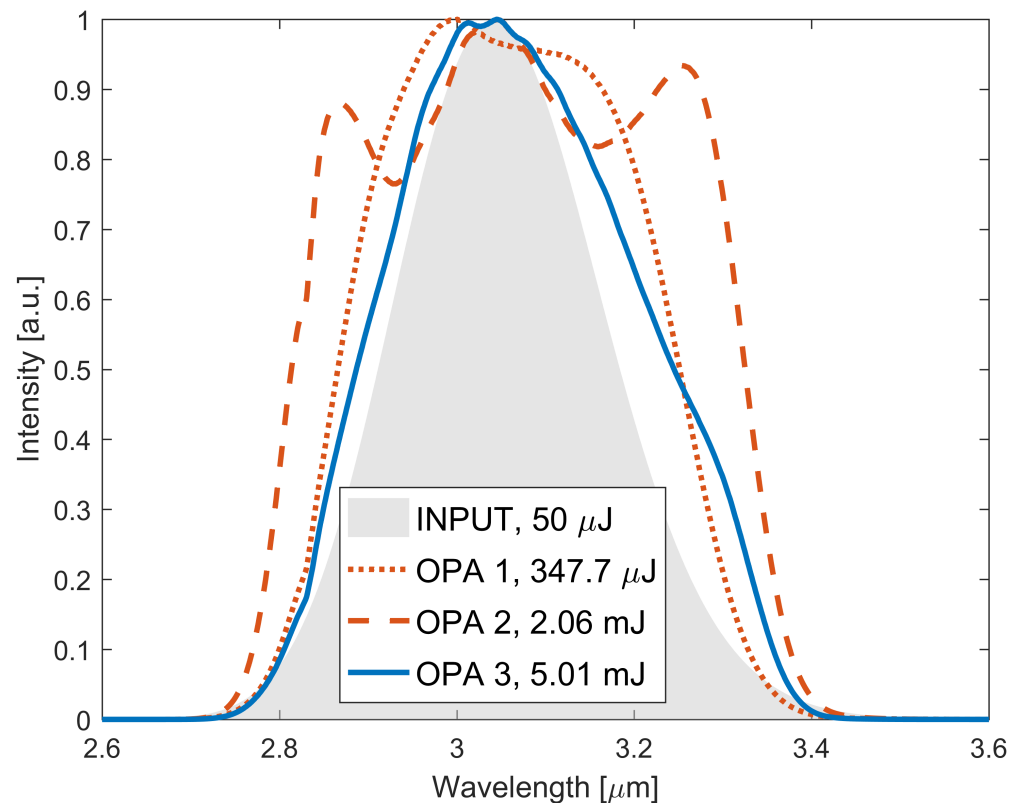


**Figure 4.** Spectra and energy output of proposed few-cycle, few-mJ-level OPCPA chain: input (shaded), OPA 1 (dotted red), OPA 2 (dashed red), and OPA 3 (blue). The final 5 mJ output represents a net 8.4% pump to signal conversion efficiency and a net gain of  $100\times$ , with an equivalent 52 fs FTL pulse length.

**Table 3.** Amplification parameters and output values of the proposed three OPCPA stage configuration.

| Stage                         | OPA1   | OPA2 | OPA3  |
|-------------------------------|--------|------|-------|
| Crystal                       | MgO:LN | KTA  |       |
| Crystal length (mm)           | 3.6    | 2    | 1.4   |
| Phase matching angle $\theta$ | 46.7°  |      | 41.6° |
| Non-collinear angle $\alpha$  | 5.1°   |      | –     |
| Pump energy (mJ)              | 4      | 16   | 40    |
| Output energy (mJ)            | 0.35   | 2.06 | 5.01  |
| Equivalent FTL duration (fs)  | 53     | 47   | 52    |

This non-linear amplification chain delivers a well behaved beam profile and shows potential compressibility to 89 fs duration using simple bulk material compression, in this case sapphire which presents larger negative group velocity dispersion at 3  $\mu\text{m}$  ( $-549.80 \text{ fs}^2/\text{mm}$  [30]) than comparable media, such as yttrium aluminium garnet (YAG,  $-360.50 \text{ fs}^2/\text{mm}$  [31]) or calcium fluoride ( $-107.02 \text{ fs}^2/\text{mm}$  [32]). These materials also have a low non-linear refractive index, which is important when compressing multi-mJ-level pulses to few-cycle duration. A careful compensation of the second and third order dispersions could allow for compression to 53 fs (see Figure 5), close to its FTL duration.

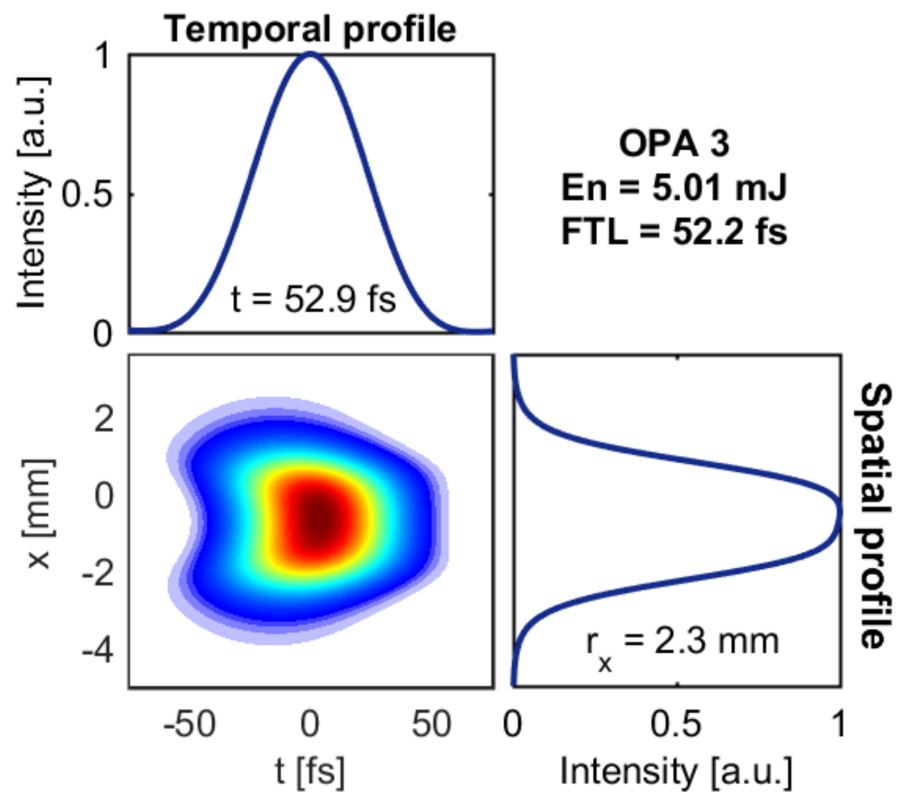


**Figure 5.** Spacetime profile of the optimized final output pulse from the hybrid OPCPA. The top and right lineouts represent the temporal and spatial profiles, respectively.

#### 4. Analysis and Discussion

The results above show that it is feasible to achieve a 5 mJ, 50 fs output pulse in a simple configuration scheme, corresponding to a total gain of  $100\times$  and a total efficiency of 8.4% which is a remarkable figure for an OPCPA in this wavelength region. Should a higher efficiency be required, a dual-chirp optical parametric amplification (DC-OPA) could be used instead, an approach that was recently demonstrated through numerical simulations as a path to achieve 5.8 mJ, 20.4 fs, 3.2  $\mu\text{m}$  with three MgO:LN DC-OPA to amplify a seed derived from a difference frequency generation (DFG) stage in KTA, showing a total conversion efficiency of  $\sim 19\%$  [33]. However, the DC-OPA would require a spectral broadened pump at the cost of a more complex configuration.

In order to compare our results with others published in the recent literature for mJ-level laser systems around 3  $\mu\text{m}$ , we compile in Table 4 the operating parameters for a few comparable systems. We can infer that, broadly, two different concepts have been demonstrated, the first based on using high-energy, 10 Hz repetition rate pump laser, such as a joule-level Ti:sapphire or Nd:YAG amplifier [15,16] and the second relying on diode-pumped ytterbium-based amplifiers operating at the kHz level [17,18]. Our approach of using different crystals potentially allows a high efficiency at a moderate pump power, while simultaneously preserving enough bandwidth for pulse compression to the shortest pulse duration reported. For instance, considering a pump based on a kW-level thin-disk Yb:YAG amplifier delivering 100 mJ, 1 ps pulses at 1 kHz we could potentially obtain simultaneously a high output energy and a few-cycle pulse duration, making this approach a very interesting alternative to existing systems.

For the simulations we assumed a number of usual simplifications, either due to limitations of the code itself or in the choice of initial conditions. These include the choice of an ideal Gaussian seed and pump pulse, both in terms of the spatial and temporal profiles, and neglecting losses and eventual distortions induced by dispersive elements and other optical components.

**Table 4.** Comparative parameters for selected mJ-level laser systems at 3 μm, ordered by output pulse energy.  $\lambda_c$  is the central wavelength,  $E_p$  the pump energy,  $E_{out}$  the output energy,  $t_{out}$  the output pulse duration, and RR the pulse repetition rate.

| Refs. | $\lambda_c$ | $E_p$ (mJ) | $E_{out}$ (mJ) | $t_{out}$ (fs) | RR (kHz) | Medium                 | Eff. (%) |
|-------|-------------|------------|----------------|----------------|----------|------------------------|----------|
| [15]  | 3.3         | 630        | 21             | 70             | 0.01     | MgO:LiNbO <sub>3</sub> | 3.3      |
| [16]  | 3.4         | 900        | 13.3           | 111            | 0.01     | LiNbO <sub>3</sub>     | 1.5      |
| [17]  | 3.0         | 25         | 2.7            | 50             | 10       | PPLN + KTA             | 10.8     |
| [18]  | 3.1         | 27         | 0.85           | 420            | 1        | MgO:PPLN               | 3.2      |
| [19]  | 2.8         | 12         | 0.52           | 100            | 1        | BBO + KTA              | 4.4      |

On the other hand, the deliberately conservative chosen parameters for these simulations, as the KTA size and the LIDT value for MgO:LN limit the calculated output, which may be exceeded in an optimized setup. The same happens with the defined chirp value of the pump and seed chosen here to allow for a straightforward compact bulk compression solution and avoid gain narrowing. Finally, considering an initial 100-mJ-level pump of which only 60 mJ are used leaves margin for additional amplification chain, e.g., with a fourth KTA stage, although at the cost of a compromised amplified bandwidth.

We analyzed the acceptance of larger bandwidths by simulating a single MgO:LN-based amplification stage with the same parameters as in Section 3.1, i.e., the same seed (but different bandwidth), same pump (16 mJ energy, corresponding to 25 GW/cm<sup>2</sup>) and same amplification geometry (Type I,  $\theta = 46.7^\circ$  and  $\alpha = 5.1^\circ$ ) for a crystal length of 2.3 mm. The seed bandwidth was varied to correspond to 40 fs and 30 fs, in order to allow comparing with the previously obtained results for 50 fs (Figure 6). The same conservative approach of having a good quality output profile was maintained. Although the bandwidths of the 50 fs and 40 fs pulses are still fully accepted by the crystal, delivering an output pulse duration (energy) of, respectively, 51 fs (1.12 mJ) and 43 fs (1.09 mJ), the 30 fs pulse is broadened to 36 fs (20% increase) with an energy of 1.02 mJ. Therefore, for pulses equal or shorter than ~3-optical cycles a thinner crystal will be required, while also slightly compromising its output energy. Calculating the bandwidth acceptance for this geometry and crystal length yields 430 nm, which reinforces these conclusions.

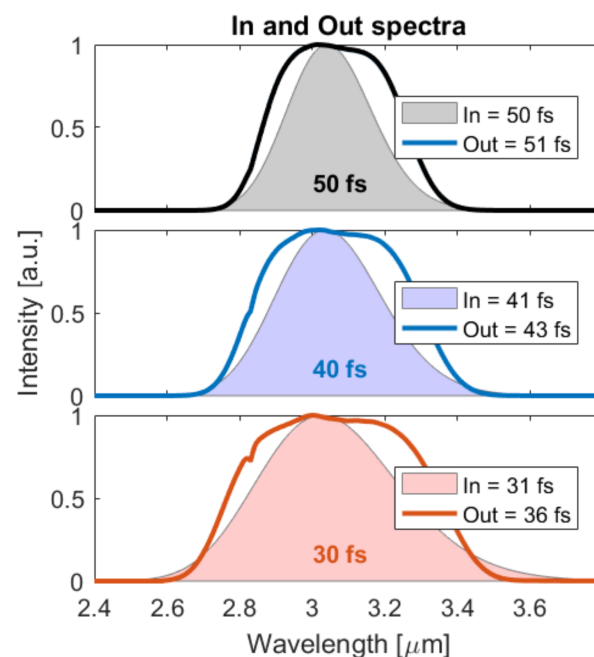


**Figure 6.** Input (shaded) and output (solid line) spectra for different seed bandwidths in a single MgO:LN-based amplification stage. (Top) 50 fs, (Center) 40 fs; (Bottom) 30 fs pulse durations.

Finally, we also simulated the output vs. input energy with corresponding crystal length that allows optimum compromise between output energy, bandwidth and beam profile (Figure 7). These outputs show preservation of the FTL duration (50 fs). This shows an approximately constant pump to pulse conversion efficiency between 4 mJ and 12 mJ ( $\sim 8.5\%$ ), dropping to 7% at 16 mJ. This strengthens our approach of using the first stage of the chain at lower energy (4 mJ) and the second stage at maximum intensity for higher gain.

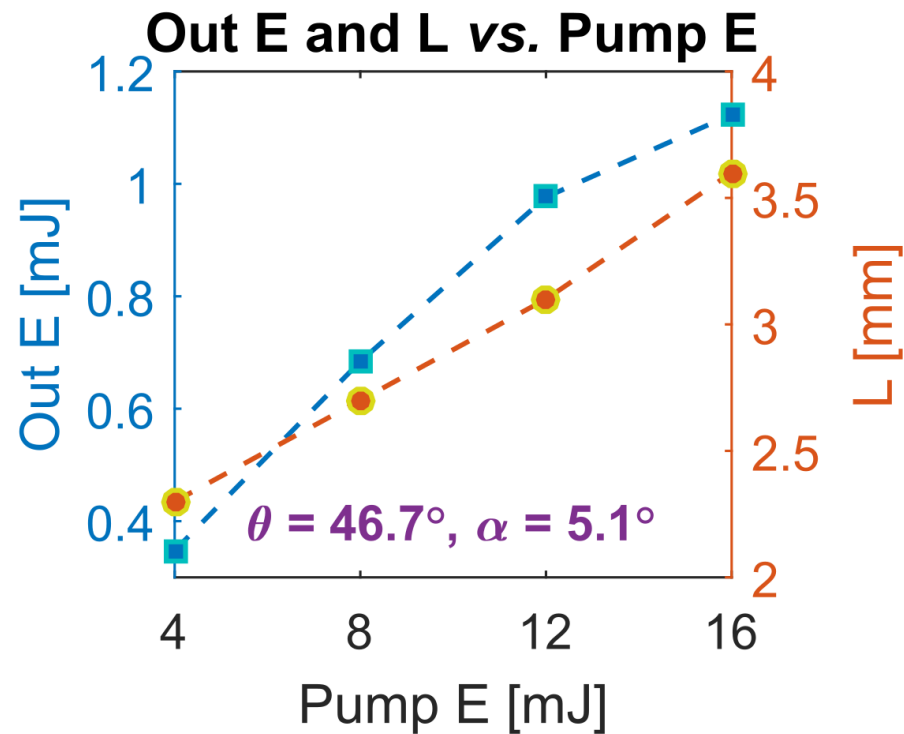


**Figure 7.** Output energy vs. pump input energy and corresponding crystal length with output FTL durations of 50 fs in a single MgO:LN-based amplification stage.

A possible implementation of the proposed amplification can be seen in Figure 8. The first part is based, e.g., on available commercial configurations consisting of a main pump system delivering 1 W, 1 kHz, 1 ps pulses at  $1.03 \mu\text{m}$  from which 75% of the energy drives a  $\sim 3 \mu\text{m}$ , 1 kHz OPCPA delivering carrier-envelope phase stable (CEP) output pulses with  $50 \mu\text{J}$ , 50 fs. The remaining pump pulse goes through a pulse picker with high extinction ratio and is stretched to 250 ps in a chirped volume Bragg grating (CVBG). The stretched signal is used to seed a diode-pumped, ytterbium-based multipass amplifier, where the  $\mu\text{J}$ -level pulses are boosted to 100 mJ at 10 Hz. This output is then compressed to 6 ps in a double-passed grating setup and the resulting 75 mJ from which 60 mJ are used and successively split into 4 mJ, 16 mJ and 40 mJ for each of the OPA stages. The mid-IR signal should be stretched to  $1/3$  of the pump pulse duration by using an adequate bulk silicon slab with anti-reflection coating. This is followed by an ultrafast fast shutter that reduces the repetition rate to that of the pump laser. Stages OPA1 and OPA2 are non-colinear, MgO:LN-based amplifiers pumped with 4 mJ and 16 mJ, respectively, and delivering  $350 \mu\text{J}$  and 2 mJ. OPA3 is a collinear amplifier pumped with 40 mJ, bringing the signal up to 5 mJ. The output pulses are compressed to 89 fs by using bulk sapphire. Both bulk materials are considered to be coated for the  $3 \mu\text{m}$  and on a single pass configuration in order to allow for negligible losses. Control of the third-order dispersion terms using, e.g., a silicon prism pair stretcher (instead of simple bulk) or an acousto-optic modulator will allow to compress the pulses to their FTL duration, however at a cost in energy of the seed.

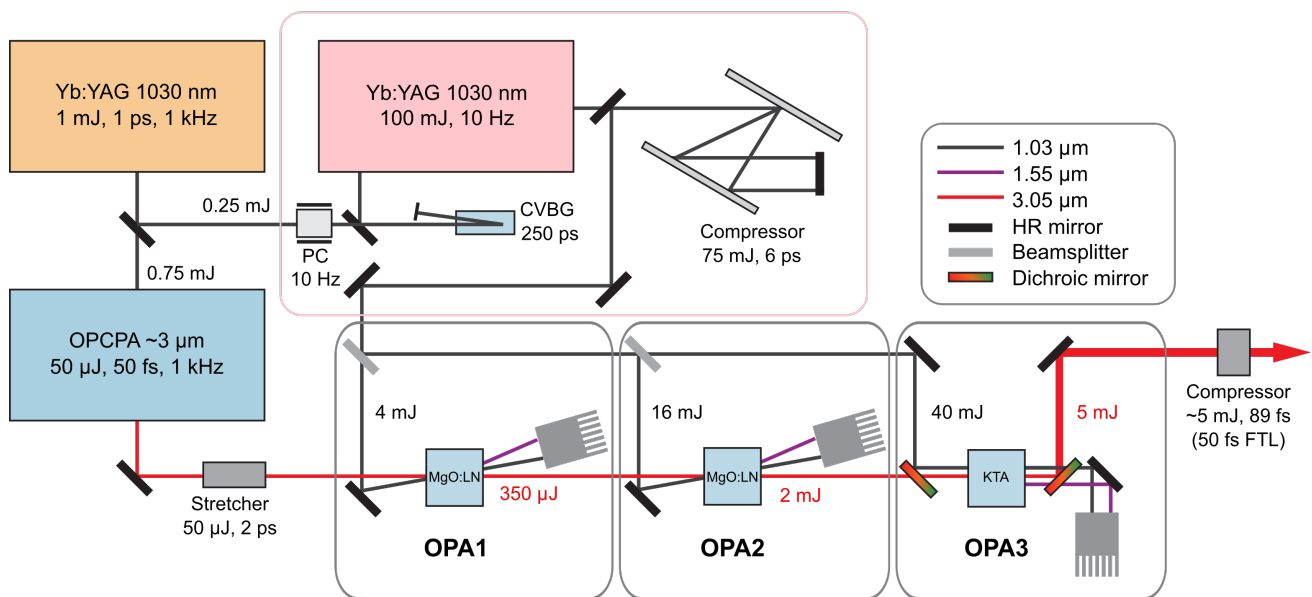


**Figure 8.** Overall schematic of a 5 mJ, 5-optical-cycles, 3  $\mu\text{m}$  mid-IR OPCPA laser system.

## 5. Conclusions

In conclusion, we have performed detailed numerical simulations for the energy scaling of 3  $\mu\text{m}$  laser pulses from the tens of  $\mu\text{J}$  to the multi-mJ level in single, double and triple-stage OPCPA setups. We show that up to 5 mJ, 5-cycle pulses can be achieved by a single stage configuration, either collinear or non-collinear, with reduced demand on the compression scheme. Through combination of two of the most promising crystals for mJ-level amplification, MgO:LN and KTA, we can further scale the energy to the multi-mJ level while preserving the few-cycle duration of the seed pulse. We conceptually propose a three-stage hybrid OPCPA combining the high amplification capability of MgO:LN and the high LIDT of KTA pumped by a 1.03  $\mu\text{m}$ , 60 mJ, ps-level Yb-based CPA, to amplify 50  $\mu\text{J}$ , 50 fs pulses to 5 mJ, 52 fs (FTL), with 8.4% total efficiency and a total gain of 100. It should be noted that in this work we use conservative values for the size of KTA taking into account the preservation of a high homogeneity. Using crystals with larger apertures and higher LIDT would allow further scaling of this systems. The development of multi-mJ, few-cycle laser systems in the mid-infrared will open the way to a new experimental regime in the investigation of processes such as high harmonic generation, broadband X-ray sources, and laser wakefield acceleration.

**Author Contributions:** Conceptualization, J.A., H.P., C.P.J. and G.F.; methodology, J.A. and H.P.; validation, J.A.; formal analysis, J.A.; investigation, J.A. and H.P.; writing—original draft preparation, J.A.; writing—review and editing, J.A., H.P., C.P.J. and G.F.; supervision, H.P. and G.F.; project administration, G.F.; funding acquisition, G.F. All authors have read and agreed to the published version of the manuscript.

**Funding:** This project has received funding from Fundação para a Ciência e Tecnologia under grant PD/BD/135177/2017 and Laserlab Portugal (National Roadmap of Research Infrastructures, PINFRA/22124/2016); European Union’s Horizon 2020 research and innovation programme under grant agreement no. 871124 (Laserlab-Europe); it was carried out in the framework of the Advanced Program in Plasma Science and Engineering (sponsored by Fundação para a Ciência e Tecnologia under grant No. PD/00505/2012) at Instituto Superior Técnico.

**Institutional Review Board Statement:** Not applicable.

**Informed Consent Statement:** Not applicable.

**Data Availability Statement:** All relevant data is within the present manuscript.

**Conflicts of Interest:** The authors declare no conflict of interest.

## References

1. Tian, K.; He, L.; Yang, X.; Liang, H. Mid-infrared few-cycle pulse generation and amplification. *Photonics* **2021**, *8*, 290.
2. Popmintchev, T.; Chen, M.C.; Popmintchev, D.; Arpin, P.; Brown, S.; Ališauskas, S.; Andriukaitis, G.; Balčiūnas, T.; Mücke, O.D.; Pugžlys, A.; et al. Bright coherent ultrahigh harmonics in the keV X-ray regime from mid-infrared femtosecond lasers. *Science* **2012**, *336*, 1287–1291. [[PubMed](#)]
3. Ghimire, S.; Reis, D.A. High-harmonic generation from solids. *Nat. Phys.* **2018**, *15*, 10–16.
4. Young, L.; Ueda, K.; Gühr, M.; Bucksbaum, P.H.; Simon, M.; Mukamel, S.; Rohringer, N.; Prince, K.C.; Masciovecchio, C.; Meyer, M.; et al. Roadmap of ultrafast X-ray atomic and molecular physics. *J. Phys. B At. Mol. Opt. Phys.* **2018**, *51*, 032003.
5. Hernández-García, C.; Popmintchev, T.; Murnane, M.M.; Kapteyn, H.C.; Plaja, L.; Becker, A.; Jaron-Becker, A. Isolated broadband attosecond pulse generation with near- and mid-infrared driver pulses via time-gated phase matching. *Opt. Express* **2017**, *25*, 11855–11866. [[PubMed](#)]
6. Chang, Z.; Corkum, P.B.; Leone, S.R. Attosecond optics and technology: Progress to date and future prospects [Invited]. *J. Opt. Soc. Am. B* **2016**, *33*, 1081.
7. Woodbury, D.; Feder, L.; Shumakova, V.; Gollner, C.; Schwartz, R.; Miao, B.; Salehi, F.; Korolov, A.; Pugžlys, A.; Baltuška, A.; et al. Laser wakefield acceleration with mid-IR laser pulses. *Opt. Lett.* **2018**, *43*, 1131–1134.
8. Pires, H.; Baudisch, M.; Sanchez, D.; Hemmer, M.; Biegert, J. Ultrashort pulse generation in the mid-IR. *Prog. Quantum Electron.* **2015**, *43*, 1–30.
9. Ma, C.; Wang, C.; Gao, B.; Adams, J.; Wu, G.; Zhang, H. Recent progress in ultrafast lasers based on 2D materials as a saturable absorber. *Appl. Phys. Rev.* **2019**, *6*, 041304.
10. Jiang, T.; Yin, K.; Wang, C.; You, J.; Ouyang, H.; Miao, R.; Zhang, C.; Wei, K.; Li, H.; Chen, H.; et al. Ultrafast fiber lasers mode-locked by two-dimensional materials: Review and prospect. *Photonics Res.* **2020**, *8*, 78.
11. Thiré, N.; Maksimenka, R.; Kiss, B.; Ferchaud, C.; Gitzinger, G.; Pinoteau, T.; Jousset, H.; Jarosch, S.; Bizouard, P.; Di Pietro, V.; et al. Highly stable, 15 W, few-cycle, 65 mrad CEP-noise mid-IR OPCPA for statistical physics. *Opt. Express* **2018**, *26*, 26907. [[PubMed](#)]
12. Elu, U.; Baudisch, M.; Pires, H.; Tani, F.; Frosz, M.H.; Köttig, F.; Ermolov, A.; St. J. Russell, P.; Biegert, J. High average power and single-cycle pulses from a mid-IR optical parametric chirped pulse amplifier. *Optica* **2017**, *4*, 1024.
13. Mero, M.; Petrov, V. High-power, few-cycle, angular dispersion compensated mid-infrared pulses from a noncollinear optical parametric amplifier. *IEEE Photonics J.* **2017**, *9*, 1–8. [[CrossRef](#)]
14. Archipovaite, G.M.; Petit, S.; Delagnes, J.C.; Cormier, E. 100 kHz Yb-fiber laser pumped 3  $\mu\text{m}$  optical parametric amplifier for probing solid-state systems in the strong field regime. *Opt. Lett.* **2017**, *42*, 891–894.
15. Fu, Y.; Xue, B.; Midorikawa, K.; Takahashi, E.J. TW-scale mid-infrared pulses near 3.3  $\mu\text{m}$  directly generated by dual-chirped optical parametric amplification. *Appl. Phys. Lett.* **2018**, *112*, 241105. [[CrossRef](#)]
16. Zhao, K.; Zhong, H.; Yuan, P.; Xie, G.; Wang, J.; Ma, J.; Qian, L. Generation of 120 GW mid-infrared pulses from a widely tunable noncollinear optical parametric amplifier. *Opt. Lett.* **2013**, *38*, 2159–2161.
17. Zou, X.; Li, W.; Qu, S.; Liu, K.; Li, H.; Wang, Q.J.; Zhang, Y.; Liang, H. Flat-top pumped multi-millijoule mid-infrared parametric chirped-pulse amplifier at 10 kHz repetition rate. *Laser Photonics Rev.* **2021**, *15*, 2000292. [[CrossRef](#)]
18. Wang, S.; Gerrity, M.; Backus, S.; Murnane, M.M.; Kapteyn, H.C.; Cousin, S.L. Multi-mJ, 1 kHz, 3.1  $\mu\text{m}$  OPCPA. In Proceedings of the Conference on Lasers and Electro-Optics, San Jose, CA, USA, 14–19 May 2017; Optical Society of America: San Diego, CA, USA, 2017; p. STh1L.5.
19. He, H.; Wang, Z.; Hu, C.; Jiang, J.; Qin, S.; He, P.; Zhang, N.; Yang, P.; Li, Z.; Wei, Z. 520- $\mu\text{J}$  mid-infrared femtosecond laser at 2.8  $\mu\text{m}$  by 1-kHz KTA optical parametric amplifier. *Appl. Phys. B* **2018**, *124*, 31.
20. Andriukaitis, G.; Balčiūnas, T.; Ališauskas, S.; Pugžlys, A.; Baltuška, A.; Popmintchev, T.; Chen, M.C.; Murnane, M.M.; Kapteyn, H.C. 90 GW peak power few-cycle mid-infrared pulses from an optical parametric amplifier. *Opt. Lett.* **2011**, *36*, 2755–2757.
21. Mitrofanov, A.V.; Sidorov-Biryukov, D.A.; Voronin, A.A.; Pugžlys, A.; Andriukaitis, G.; Stepanov, E.; Ališauskas, S.; Flöri, T.; Fedotov, A.B.; Panchenko, V.Y.; et al. Subterawatt femtosecond pulses in the mid-infrared range: new spatiotemporal dynamics of high-power electromagnetic fields. *Physics-Uspokhi* **2015**, *58*, 89.
22. Fattahi, H.; Barros, H.G.; Gorjan, M.; Nubbemeyer, T.; Alsaif, B.; Teisset, C.Y.; Schultze, M.; Prinz, S.; Haefner, M.; Ueffing, M.; et al. Third-generation femtosecond technology. *Optica* **2014**, *1*, 45–63.
23. Alismail, A.; Wang, H.; Barbiero, G.; Altwaijry, N.; Hussain, S.A.; Pervak, V.; Schweinberger, W.; Azzeer, A.M.; Krausz, F.; Fattahi, H. Multi-octave, CEP-stable source for high-energy field synthesis. *Sci. Adv.* **2020**, *6*, eaax3408.
24. Lang, T.; Harth, A.; Matyschok, J.; Binhammer, T.; Schultze, M.; Morgner, U. Impact of temporal, spatial and cascaded effects on the pulse formation in ultra-broadband parametric amplifiers. *Opt. Express* **2013**, *21*, 949.
25. Petrov, V.; Noack, F.; Stolzenberger, R. Seeded femtosecond optical parametric amplification in the mid-infrared spectral region above 3  $\mu\text{m}$ . *Appl. Opt.* **1997**, *36*, 1164–1172.
26. Petrov, V.; Noack, F. Mid-infrared femtosecond optical parametric amplification in potassium niobate. *Opt. Lett.* **1996**, *21*, 1576–1578. [[PubMed](#)]
27. Baudisch, M.; Hemmer, M.; Pires, H.; Biegert, J. Performance of MgO:PPLN, KTA, and KNbO<sub>3</sub> for mid-wave infrared broadband parametric amplification at high average power. *Opt. Lett.* **2014**, *39*, 5802.

28. Furukawa, Y.; Kitamura, K.; Alexandrovski, A.; Route, R.; Fejer, M.; Foulon, G. Green-induced infrared absorption in MgO doped LiNbO<sub>3</sub>. *Appl. Phys. Lett.* **2001**, *78*, 1970–1972.
29. Bach, F.; Mero, M.; Chou, M.H.; Petrov, V. Laser induced damage studies of LiNbO<sub>3</sub> using 1030-nm, ultrashort pulses at 10–1000 kHz. *Opt. Mater. Express* **2017**, *7*, 240–252.
30. Malitson, I.H.; Dodge, M.J. Refractive-index and birefringence of synthetic sapphire. *J. Opt. Soc. Am.* **1972**, *62*, 1405–1405.
31. Zelmon, D.E.; Small, D.L.; Page, R. Refractive-index measurements of undoped yttrium aluminum garnet from 0.4 to 5.0 μm. *Appl. Opt.* **1998**, *37*, 4933–4935.
32. Li, H. Refractive index of alkaline earth halides and its wavelength and temperature derivatives. *J. Phys. Chem. Ref. Data* **1980**, *9*, 161–290.
33. Yin, Y.; Li, J.; Ren, X.; Wang, Y.; Chew, A.; Chang, Z. High-energy two-cycle pulses at 3.2 μm by a broadband-pumped dual-chirped optical parametric amplification. *Opt. Express* **2016**, *24*, 24989–24998. [[PubMed](#)]